Neuroscience 167 (2010) 1–10

RAPID REPORT

FUNCTIONAL AND HISTOLOGICAL PROPERTIES OF CAUDAL INTRAPARIETAL AREA OF MACAQUE MONKEY

N. KATSUYAMA,[a]* A. YAMASHITA,[a] K. SAWADA,[a] T. NAGANUMA,[a] H. SAKATA[a,b] AND M. TAIRA[a,c]

[a]*Division of Applied System Neuroscience, Department of Advanced Medical Science, Nihon University School of Medicine, Itabashi, Tokyo 173-8610, Japan*

[b]*Department of Administrative Nutrition, Tokyo Seiei College, Katsushika, Tokyo 124-8530, Japan*

[c]*Advanced Research Institute for the Science and Humanities, Nihon University, Chiyoda, Tokyo 102-8251, Japan*

Abstract—In our previous studies, we found that cells in the caudal intraparietal (CIP) area of the macaque monkey selectively responded to three-dimensional (3D) features, such as the axis and surface orientations, and we suggested that this area played a crucial role in 3D vision. In this study, we investigated (1) whether cells in CIP respond to other 3D features, such as curvature, and (2) whether CIP has any histological property to distinguish it from neighboring areas. Curvatures defined by a random-dot stereogram were presented on a display while the monkey performed a fixation task. The shape and amount of curvature were manipulated by two independent variables, shape index and curvedness, respectively. Two-way ANOVA showed that 19 out of 56 visually responsive cells (34.0%) showed the main effect of shape index. We tentatively designated these cells as 3D curvature-selective (3DCS). Of these, six 3DCS cells showed the main effects of shape index and curvedness, whereas 13 showed the main effect of shape index only. In both types of 3DCS cells, preferred shape indices calculated from tuning curves at two levels of curvedness matched well. These results indicate that the majority of 3DCS cells responded equally to a particular shape of curvatures with different curvedness levels. An immunohistochemical study showed that the recording sites of 3DCS cells were in a cortical region characterized by a dense SMI-32 immunoreactivity in the caudal portion of the lateral intraparietal sulcus (IPS), which suggests that this region is comparable to the lateral occipital parietal (LOP) designated in the caudal IPS previously. Further investigations showed that this region was separated from LIPv, the ventral subdivision of lateral intraparietal (LIP) located rostral to CIP/LOP. These results suggest that CIP is a cortical area distinct from LIP histologically as well as functionally.

*Corresponding author. Tel: +81-3-3972-8111, ext. 2231; fax: +81-3-3972-8292.
E-mail address: katz@med.nihon-u.ac.jp (N. Katsuyama).

Abbreviations: AIP, anterior intraparietal; CDI, curvature discrimination index; CIP, caudal intraparietal; CPSI, calculated preferred shape index; CSI, curvature selectivity index; DAB, diaminobenzidine tetrahydrochloride; DB, dorsal band; IPS, intraparietal sulcus; LIP, lateral intraparietal; LIPd, dorsal subdivision of LIP; LIPv, ventral subdivision of LIP; LOP, lateral occipital parietal; PB, phosphate buffer; POS, parieto-occipital sulcus; VB, ventral band; VR, visually responsive; 3D, three-dimensional; 3DCS, 3D curvature-selective.

Key words: curvature, SMI-32, parietal cortex, CIP, 3D vision, macaque monkey.

The intraparietal sulcus (IPS) of the macaque monkey is divided into many cortical areas. Our previous studies revealed that cells in the caudal portion of the lateral bank of IPS selectively respond to three-dimensional (3D) structures of visual stimuli, such as the axis orientation (Kusunoki et al., 1993; Sakata et al., 1998) and surface orientation (Taira et al., 2000; Tsutsui et al., 2002). This region was designated as area cIPS or c-IPS (Sakata et al., 1998), and later CIP (Taira et al., 2000). These findings strongly suggest that CIP is a cortical area for the processing of 3D structures of objects. Studies of computational theory have suggested that the surface orientations of planes and curvatures are critical for the representation of 3D shapes in our visual system (Marr, 1982). Thus, if CIP is the processing center for 3D structure cognition, CIP cells may also respond to curvatures.

Although we designated the caudal portion of the lateral IPS as CIP, it was defined functionally, and it is unclear whether CIP has a specific histological property. Lewis and Van Essen (2000) examined the architectonic organization of the posterior parietal cortex by immunohistochemical staining using SMI-32 antibody. They found a cortical region characterized by the presence of a dense band of SMI-32 immunoreactivity in the caudal portion of the lateral bank of IPS and designated this region as the lateral occipital parietal (LOP). We speculated that LOP identified by Lewis and Van Essen (2000) might be homologous to CIP, because their geographic location in the caudal IPS was comparable.

In this study, we determined whether cells in CIP also responded to other 3D features, such as curvature, and investigated whether CIP where we recorded such cells could be characterized histologically as well by examining the immunohistochemical organization in the caudal portion of the lateral IPS using SMI-32 antibody.

EXPERIMENTAL PROCEDURES

Materials and apparatus

A male Japanese monkey (monkey GI, *Macaca fuscata*, 5 years old, 6 kg) was used for neuronal recording and immunohistochemical study. Because a portion of the brain tissue was damaged by long-term neuronal recordings, we utilized immunohistochemical samples from another three monkeys (monkeys M17, M19, and HG, *Macaca fuscata*, young adults, 3–6 kg) prepared for other anatomical studies.

0306-4522/10 $ - see front matter © 2010 IBRO. Published by Elsevier Ltd. All rights reserved.
doi:10.1016/j.neuroscience.2010.01.028

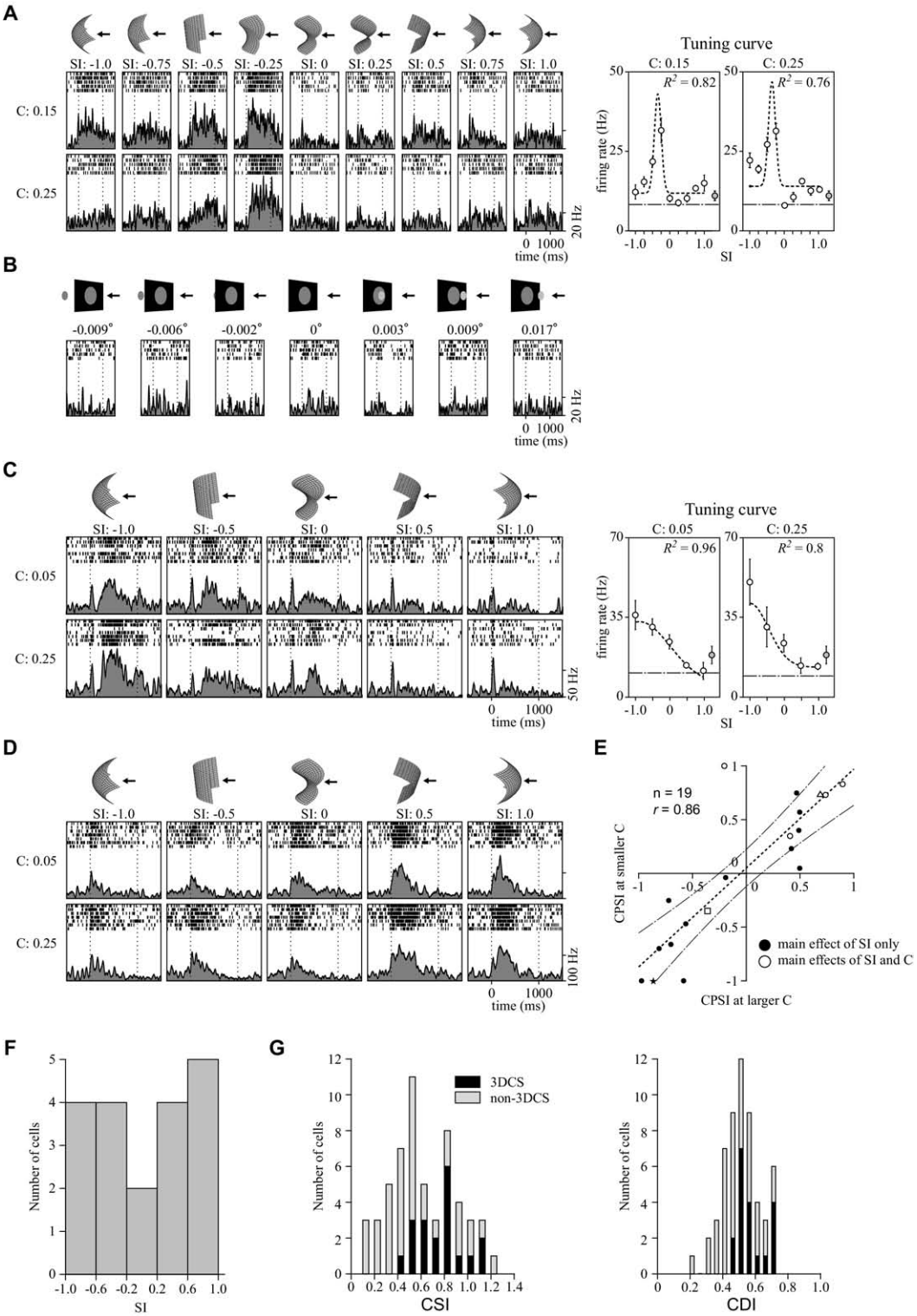

Fig. 1. (A) (C Left): example of a 3DCS cell responding to concave curvatures. This cell was tested using nine shapes (S: −1.0, −0.75, −0.5, −0.25, 0, 0.25, 0.5, 0.75, 1.0) at two curvedness levels (C: 0.15 and 0.25). Schematic diagrams of curvatures tested are shown on the histograms. Arrows indicate the direction of the viewpoint to each stimulus. (C Right): tuning curves of this cell at two curvedness levels. Gaussian function (indicated by dotted line) was fitted to the responses of the cell. The goodness of the curve fitting was indicated by the coefficient of determination (R^2). The CPSIs of this cell at the smaller curvedness and larger curvedness were −0.36 and −0.35, respectively. The gray circles in the tuning curves represent the responses to the front parallel plane. The broken lines indicate the mean firing rates of spontaneous activity. (B) Responses of 3DCS cells shown in (A) to disparity patches presented at seven positions across a depth over the fixation target. Schematic diagrams showing the positions of the disparity patches (small gray circles) and values of disparity are shown on the histograms. Arrows indicate the direction of the viewpoint to each stimulus. The diameter of the

This study was approved by the Experimental Animal Committee of Nihon University Medical School (approval number: 020146/2002). The animals were treated in accordance with the National Institutes of Health Guide for the Care and Use of Laboratory Animals.

Physiological procedures

Behavioral task. The monkey was trained in a fixation task. When a fixation target (a red circle, 0.2° in diameter) was presented at the center of the display, the monkey was required to press a key and to fixate on the target. After a variable duration (1000–1250 ms), a visual stimulus was presented over the fixation target for 1 s, followed by another variable duration (1000–1250 ms). The monkey had to maintain fixation throughout the presentation of the stimulus and was rewarded with a drop of juice if he released the key when the fixation target was turned off. The movements of one eye were continuously monitored by an infrared eye tracking system with a CCD camera (R-21C-AS, RMS Hirosaki, Hirosaki, Japan) at a sampling rate of 250 Hz. When the eye position exceeded the limit of 1 degree from the fixation target, the trial was immediately aborted.

Visual stimuli. All visual stimuli were generated by software for 3D graphics (Omega Space ver. 2.0, Solidray Institute, Yokohama, Japan) and presented on a display (21 inches, 2048×1024 pixels) with a liquid crystal polarized filter (Nu210544, MacNaughton Inc., Beaverton, OR, USA). The display was placed 85.5 cm in front of the monkey's eyes. The filter was switched at 120 Hz, and 60 frames/s of stimulus were presented to each eye. The monkey wore a pair of polarized glasses to view these stimuli stereoscopically. Images of 3D curvatures were generated by expressions proposed by Koenderink (Koenderink, 1990; de Vries et al., 1993). A series of curvatures can be represented by manipulating the principal curvature (K), which defines the curvature of a local patch over quadratic surfaces. Using the maximum (K_{max}) and minimum (K_{min}) values of the principal curvature, shape index and curvedness are defined by the following expressions.

$$\text{Shape index} = -\frac{2}{\pi}\arctan\frac{K_{max}+K_{min}}{K_{max}-K_{min}}$$

$$\text{Curvedness} = \sqrt{\frac{K_{max}^2+K_{min}^2}{2}}$$

Shape index defines the shape of curvatures. It can take values from −1 to 1, and enables us to place curvatures on a continuous one-dimensional scale. The scale can be divided into surface types: from −1.0 to −0.5, concave ellipsoidal; from −0.5 to 0.5, hyperbolic shapes (saddles); and from 0.5 to 1.0, convex ellipsoidal (see schematic diagrams in Fig. 1A, B). The boundaries at −0.5 and 0.5 are the cylinders of a concave and a convex, respectively. Curvedness is the amount of curvature. It can vary from 0 (flat surfaces) to infinity (needles). It has been shown that these quantities can provide a convenient parameterization for psychophysical tests for human subjects (de Vries et al., 1993). In the first half of the physiological study, cells were tested with five shape indices (SI = −1.0, −0.5, 0, 0.5, 1.0) at two curvedness levels (C=0.05 and 0.25). The maximum disparities of curvatures at C=0.25 around the fixation target was 0.016°. This corresponded to 24.1 cm from the fixation target toward the observer, and was almost the limit of binocular fusion for 3D vision in the settings employed in this study. Likewise, the maximum disparities of curvatures around the fixation target at C=0.15 and 0.05 were 0.008° and 0.002°, which corresponded to 14.4 and 4.8 cm from the fixation target toward the observer, respectively. As shown in Fig. 1D, vigorous responses were evoked at two shape indices in some cells. We considered that five shape indices might be crude to test selectivity for the shape index of CIP cells, and added another four shape indices (SI=−0.75, −0.25, 0.25, and 0.75) to fill the gaps between the five shape indices in the second half of the physiological study. In addition, because some CIP cells showed weak responses to a curvedness level of 0.05, we employed a larger curvedness in the second half of the physiological study (C=0.15 and 0.25). Fifty-six cells were tested with five shape indices at curvedness levels of 0.05 and 0.25, and forty-two cells were tested with nine shape indices at curvedness levels of 0.15 and 0.25. Because the contour of curvatures projected on the display varied with the stimulus presented, a circular window (13.3° in diameter) was attached to the surface of the display to cover the boundary of the stimuli.

We also tested responses of 3DCS cells to disparity patches. A circular patch (6.7° in diameter) was presented over the fixation target at seven positions across a depth. Each position corresponded to the maximum and minimum portions of curvatures around the fixation target at the three curvedness levels. The disparities of the seven positions were −0.009°, −0.006°, −0.002°, 0°, 0.003°, 0.009°, and 0.017°, which corresponded to −25, −15, −5, 0, 5, 15, and 25 cm from the fixation target toward the observer, respectively (see schematic diagrams in Fig. 1B).

Single-unit recording and data analysis. Before the single-unit recording, the T1-weighted anatomical images of the monkey brain were collected using a 1.5 T MRI scanner (Symphony, Siemens, Erlangen, Germany) to construct a stereotaxic atlas. For head fixation, a halolike metal ring was implanted in the monkey's skull (Isoda et al., 2005), and a recording chamber was stereotaxically implanted over IPS under sodium pentobarbital-induced anesthesia. After recovery from the surgery, tungsten microelectrodes (Frederick Haer, Bowdoinham, ME, USA) were inserted into the lateral bank of the IPS with a micromanipulator (MSD, Alpha Omega, Nazareth, Israel) for extracellular single-unit recordings in CIP. Action potentials during the behavioral task were recorded and discriminated into single-unit activity using a waveform-based spike detector (MSD, Alpha Omega, Nazareth, Israel) for off-line analysis. When the mean firing rate of a cell responding to any curvature tested within 200 ms after stimulus onset was significantly higher than that before stimulus onset, the cell was regarded as visually responsive (Mann–Whitney's U-test, $P<0.01$). The tuning of recorded cells to shape index and curvedness were

patch was 6.7°. (C) Left: another example of a 3DCS cell responding to concave ellipsoid. This cell was tested using five shapes (S: −1.0, −0.5, 0, 0.5, 1.0) at two curvedness levels (C: 0.05 and 0.25). Right: tuning curves of this cell at two curvedness levels. The CPSIs of this cell at the smaller curvedness and larger curvedness were −0.86 and −1.0, respectively. (D) Another example of a 3DCS cell responding to convex curvatures. This cell was tested using five shapes at two curvedness levels (C: 0.05 and 0.25). The CPSIs of this cell at the smaller curvedness and larger curvednesses were 0.69 and 0.74, respectively. (E) The CPSIs at the smaller curvedness levels were plotted against those at the larger curvedness (n=19). Filled symbols indicate 3DCS cells showing the significant main effect of shape index only by two-way repeated-measures ANOVA. Open symbols indicate 3DCS cells showing the main effects of shape index and curvedness. 3DCS cells shown in (A, C, D) are indicated by an open rectangle, a filled star, and an open triangle, respectively. The slope of the linear regression line (dotted line) and the correlation coefficient (r) were 0.92 and 0.86, respectively. The broken lines indicate 95% confidence limits. (F) Distribution of the best shape index of 3DCS cells. The preferred shape index at the curvedness at which the maximum response was evoked was assigned to the best shape index of the cell. (G) Distribution of CSI (left) and CDI (right) for all visually responsive cells in CIP. Filled and gray bars indicate 3DCS and non-3DCS cells, respectively. Error bars in the tuning curves in (A) and (C) indicate S.D. C, curvedness; SI, shape index.

tested by two-way repeated-measures ANOVA. In this study, we focused on the tuning profile of CIP cells responding to the shape of curvatures. For this reason, cells showing the significant main effect of shape index ($P<0.01$) that showed no interaction with curvedness ($P>0.01$) were tentatively defined as 3D curvature-selective (3DCS). Thus, cells responding to a particular shape at larger curvedness and/or smaller curvedness were selected on the basis of this definition. To quantify the tuning of 3DCS cells to shape index, Gaussian function was fitted to neuronal responses by the least-squares method using the constrained minimization tool, "fmincon," in Matlab (Mathworks, Natick, MA, USA). We employed curve fitting instead of multiple comparisons in this analysis, because shape index was a continuous variable in its definition. The calculated preferred shape index (CPSI) for each 3DCS cell was given by the shape index at which the tuning curve reached a peak. The best shape index was defined as CPSI at curvedness at which the largest response was evoked in a cell. To assess the tuning strength of a 3DCS cell with respect to shape index, curvature selectivity index (CSI) and curvature discrimination index (CDI) were calculated for each cell using the following expressions:

$$\mathrm{CSI}=\frac{R_{\max}-R_{\min}}{R_{\max}},$$

$$\mathrm{CDI}=\frac{(R_{\max}-R_{\min})}{(R_{\max}-R_{\min})+2\times RMS_{error}}$$

where $R_{\max}$ and $R_{\min}$ are the mean responses to the most and least effective stimuli, respectively. RMS_{error} is the residual variance around the means across the entire tuning curve. These indices were calculated using the square root of firing rates to homogenize the variance in firing rate (Prince et al., 2002). CSI is a conventional measure of the strength of selectivity, which compares the difference between the firing rates in response to the preferred and least-preferred shapes with the firing rates in response to the preferred shape. CSI is 1 when a cell responds only to the preferred shape and is 0 when the cell responds to the preferred and least-preferred shapes equally. CDI is an indicator for selectivity, which takes the variance in firing into account, and has been shown to be a better measure of selectivity of V1 cells to binocular disparity (Prince et al., 2002).

Reconstruction of recording sites of 3DCS cells. The recording sites of 3DCS cells were reconstructed using MR images and photomicrographs of Nissl and SMI-32 immunohistochemical stainings of the brain to compare them with the location of strong SMI-32 immunoreactivity. The shrinkage of the brain by histological processing was estimated by electric lesions made stereotaxically in the intact regions of the brain just before perfusion. The defects of the brain tissue were supplemented by superimposing MR images on the photomicrographs of the coronal sections at the corresponding rostrocaudal level. We reconstructed all electrode tracks and compared their locations with those of SMI-32 immunoreactivity in coronal plane.

Histological procedures

Histochemistry. Animals were sedated with ketamine (5.7 mg/kg body weight) and xylazine (1.5 mg/kg body weight), and anesthetized by injection of an overdose of sodium pentobarbital. After deep anesthesia was attained, intracardial perfusion of saline was performed followed by that of ice-cold 4% paraformaldehyde in 0.1 M phosphate buffer (PB, pH=7.4). After perfusion, brains were removed and cut into 2–3-cm-thick coronal blocks stereotaxically. The brain blocks were immersed in 30% sucrose in 0.1 M phosphate-buffered saline (PBS, pH=7.4) until they sank. Fifty-micrometer-thick sections were cut on a sliding microtome (Yamato Koki, Tokyo, Japan) and kept in 0.01% sodium azide in PBS at 4 °C until use. One-in-ten series of sections were used for Nissl staining (Cresyl Violet) and SMI-32 immunohistochemical staining. Free-floating sections were reacted with 0.01% H_2O_2 in methanol for 30 min at 4 °C and then thoroughly washed in PB. Following the incubation with 0.1% Triton X-100, 10% fish gelatin (Sigma, St. Louis, MO, USA) and 1% normal horse serum (Vector Laboratories, Burlingame, CA, USA) in PB (G-PB) for 2 h, the sections were reacted with the monoclonal antibody SMI-32 (Sternberger Monoclonals, Inc., Baltimore, MD, USA) at a dilution of 1:10,000 in G-PB for 48 h at 4 °C. After thoroughly washing with PB, the sections were incubated overnight in a biotinylated secondary antibody (Vector) at a dilution of 1:200 in G-PB at 4 °C and then washed with PB. The sections were reacted with a Vectastain *elite* ABC solution (Vector) for 90 min. Following the washing with 0.05 M Tris–HCl buffer (pH=7.6), the sections were incubated with 0.03% 3,3′-diaminobenzidine tetrahydrochloride (DAB, Merck, Darmstadt, Germany) in Tris–HCl buffer for 2 h at 4 °C and then reacted with DAB and 0.03% H_2O_2 in sTris–HCl buffer for 5–10 min. As described above, a portion of the brain tissue of monkey GI was damaged, and this might cause artifactually low intensities of SMI-32 immunohistochemical staining around the damaged tissues. Because the purpose of this study was to compare the pattern of SMI-32 immunohistochemical staining in the caudal IPS with the locations of recording sites of 3DCS cells, we allowed a longer time for DAB reaction in the processing of immunohistochemical samples from monkey GI to obtain an intense SMI-32 immunohistochemical staining.

Measurement of relative thickness of band of SMI-32 immunoreactivity. Dense SMI-32 immunoreactivity was observed in the lateral bank of the caudal portion of IPS. It appeared to be a dark band lying in layers II/III and V in photomicrographs at low magnification (Fig. 2A). The lower border of the band of SMI-32 immunoreactivity in layers II/III corresponded to the border between layer III and IV identified by Nissl staining. We utilized the relative thickness of the band of SMI-32 immunoreactivity in layers II/III to the full width of the supragranular layers as an index of SMI-32 immunoreactivity in a coronal section, and plotted it against the rostrocaudal levels to compare the recording sites of 3DCS cells with the rostrocaudal extent of cortex with dense SMI-32 immunoreactivity. The band of SMI-32 immunoreactivity in layers II/III was chosen in this analysis because it was thick enough to measure it as compared with thin band of SMI-32 immunoreactivity in layer V. The thickness of the band of SMI-32 immunoreactivity in layers II/III and the full width of the supragranular layers were measured using software for image analysis (Win ROOF, Mitani Corporation, Fukui, Japan). Colored photomicrographs showing SMI-32 immunoreactivity were transformed into grayscale images. The boundary between the dark band of SMI-32 immunoreactivity and the background was determined by binarization of the grayscale images using two thresholds. The density histograms of the grayscale images showed polymodal distributions. The lower threshold was set to 0 (black) in all cases, and the upper threshold was adjusted so that the lower border of the band of SMI-32 immunoreactivity in layers II/III was visible in the binarized images (see the right column in Figs. 2C and 4D). The thickness of the band of SMI-32 immunoreactivity in layers II/III and the full width of the supragranular layers in the binarized images were measured at the maximum thickness (for example, a and b in the right column of Fig. 2C). The relative thickness of the band at position i in the rostrocaudal direction (T_i) was normalized to the maximum and minimum values of T_i using the following expression to emphasize the change:

$$RT_i=100\times\frac{T_i-T_{\min}}{T_{\max}-T_{\min}},$$

where RT_i represents the normalized relative thickness of the band of SMI-32 immunoreactivity at position i in the rostrocaudal

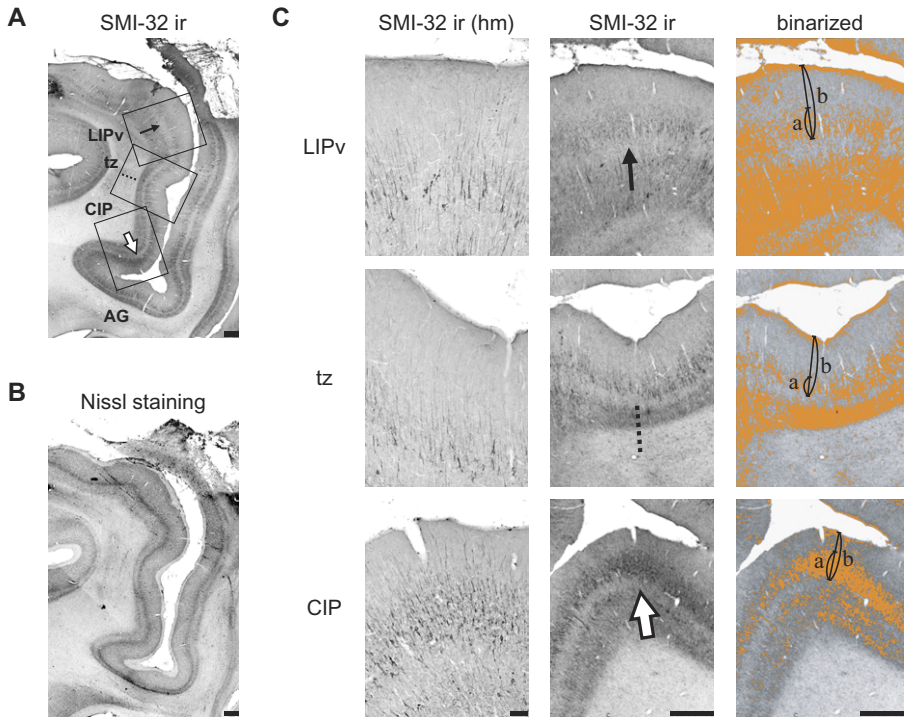

Fig. 2. (A) Photomicrograph showing SMI-32 immunoreactivity in the caudal portion of the left IPS of monkey GI. VB (CIP) and DB (LIPv) are indicated by white and thin arrows, respectively. These two areas were observed in the same coronal section and were separated by the transitional zone (indicated by a dotted line) with a thin band of SMI-32 immunoreactivity. (B) A photomicrograph of cytoarchitecture by Nissl staining (Cresyl violet). Scale bar=1 mm. (C) Left: photomicrographs showing SMI-32 immunoreactivity at high magnification. Images of LIPv, transitional zone, and CIP are shown from the top to bottom. Middle: enlarged photomicrographs indicated by rectangles in (A). Right: binarized images are superimposed on the photomicrographs shown in the middle. The thickness of the bands of SMI-32 immunoreactivity and the full width of the supragranular layers are indicated by a and b, respectively. All images are rotated so that the pia matter is on the top. Scale bar=100 μm in the left column; 1 mm in the middle and right columns. AG, annectant gyrus; hm, high magnification; ir, immunoreactivity; tz, transitional zone.

direction. $T_{max.}$ and T_{min} indicate the maximum and minimum values of T_i, respectively. RT_i was measured basically at 500 μm interval in the caudal portion of IPS and was plotted against the rostrocaudal levels.

RESULTS

Curvature-selective cells in CIP

We recorded ninety-eight cells from the caudal portion of the lateral bank of IPS from both hemispheres of the monkey. The classification of recorded cells is shown in Table 1. Among them, fifty-six cells (56/98, 57.1%) were visually responsive (VR). The responses of VR cells to shape index and curvedness were analyzed by two-way repeated-measures ANOVA. As described in the experimental procedures, we tentatively defined cells showing the main effect of shape index ($P<0.01$) without interaction ($P>0.01$) in their responses as 3D curvature-selective (3DCS) in this study. Nineteen cells (19/56, 33.9%) met this criteria. Six cells showed the main effect of curvedness only. Of the nineteen 3DCS cells, 13 cells showed the main effect of shape index only, indicating that these cells respond equally to curvatures at two curvedness levels. Other six 3DCS cells showed significant main effects of shape index and curvedness, indicating that these cells respond to 3D curvatures with specific shape index and curvedness. An example of a 3DCS cell is shown in Fig. 1A. We tested the responses of this cell to the nine shapes illustrated above the histograms at two curvedness levels (C=0.15 and 0.25). This cell showed the main effects of both shape index and curvedness. The largest response of this cell was evoked at the larger curvedness. The tuning of this cell to shape index was quantified by fitting the Gaussian curve to the responses (Fig. 1A, right). The goodness of the curve fitting was represented by coefficients of determination (R^2). Values of R^2 of this cell at the smaller curvedness and larger curvedness were 0.82 and 0.76, respectively. R^2 of all 3DCS cells was 0.83±0.16 (19 pairs, mean±SD). The CPSI was determined by shape index at the peak of the tuning curve. The values of CPSI

Table 1. Classification of cells

Category of cells	n
Visually responsive	56
Main effect of SI only[a]	13
Main effects of SI and C[a]	6
Main effect of C only	6

Numbers of cells showing the significant ($P<0.01$) main effects of SI, C, and both by two-way repeated-measures ANOVA are shown.
[a] Cells classified into these categories were defined as 3D curvature-selective. SI, shape index; C, curvedness.

of this cell at the smaller curvedness and larger curvedness were −0.36 and −0.35, respectively. We also tested the responses of this cell to disparity patches presented at the seven positions across a depth (Fig. 1B). No response to the disparity patches was elicited in this cell, although the disparities of −0.006° and −0.002° were close to those of preferred shapes around the fixation target at the larger curvedness and smaller curvedness, respectively. We tested the responses of four 3DCS cells to disparity patches. However, no 3DCS cell showed systematic responses to them. Another example of a 3DCS cell is shown in Fig. 1C. We tested the responses of this cell to the five shapes illustrated above the histograms at two curvedness levels (C=0.05 and 0.25). This cell selectively responded to the concave ellipsoid. This cell showed the main effect of shape index only. Although the response to the front parallel plane was larger than those to convex curvatures, it was significantly smaller than those to the preferred stimuli. The largest response of this cell was evoked at the larger curvedness. The values of CPSI of this cell at the smaller curvedness and larger curvedness were −0.86 and −1.0, respectively. Another example of a 3DCS cell is shown in Fig. 1D. We tested the responses of this cell to the five shapes at two curvedness levels (C=0.05 and 0.25). This cell responded to convex shapes at both curvedness levels, and the CPSIs at the smaller curvedness and larger curvedness were 0.69 and 0.74, respectively. The CPSIs of all 3DCS cells at a smaller curvedness (C=0.05 or 0.15) were plotted against those at a larger curvedness (C=0.25) in Fig. 1E. As predicted by the definition of a 3DCS cell, the CPSIs at the two levels of curvedness matched well. Statistical analysis showed that the correlation between CPSIs at two curvedness levels was significant [$P<0.001$, correlation coefficient (r)=0.86]. The slope of the linear regression line (dotted line) was 0.92, and fourteen out of nineteen 3DCS cells were inside the 95% confidence interval (indicated by broken lines).

The CPSI at the curvedness at which the largest response was obtained was assigned as the best shape index for the 3DCS cell. The distribution of the best shape indices for nineteen 3DCS cells is shown in Fig. 1F. The best shape indices were distributed in the range of nearly all shape indices tested. These results showed that some basic shapes of the 3D curvatures, such as saddles, concave or convex ellipsoid, and cylinders, are encoded in CIP.

The tuning strength of 3DCS cells to shape index was assessed using two indices. First, we calculated CSI for the responses of all VR cells to shape index at the curvedness at which the largest response was evoked (Fig. 1G, left). The mean CSIs of 3DCS and non-3DCS cells were 0.79±0.21 and 0.58±0.29 (mean±SD), respectively. The mean CSI was significantly larger in 3DCS than in non-3DCS cells [Student's t-test, $t(54)=2.81$, $P<0.01$]. Next, we calculated CDI, a selectivity index that takes the variability in the firing rate of a cell into account. The distributions of CDIs of 3DCS and non-3DCS cells are shown in Fig. 1G (right panel). The mean CDIs of 3DCS and non-3DCS cells were 0.59±0.08 and 0.50±0.11 (mean±SD), respectively. The mean CDI of 3DCS cells was significantly higher than that of non-3DCS cells [Student's t-test, $t(54)=3.11$, $P<0.01$].

SMI-32 immunohistochemistry in the caudal IPS

As described by Lewis and Van Essen (2000), a dense SMI-32 immunoreactivity was observed in the ventral portion of the lateral bank of caudal IPS (white arrow in Fig. 2A). It appeared to be a dark band lying along gray matter in coronal sections in photomicrographs at low magnification. Comparison with the adjacent section whose cytoarchitecture was revealed by Nissl staining demonstrated that the band was in layers II/III and V (Fig. 2B). Morphologically, the lateral bank of IPS appears as the "operculum" over the annectant gyrus (AG in Fig. 2A) in coronal sections of this rostrocaudal level. In this study, we refer to the dense SMI-32 immunoreactivity observed in the ventral "operculum" of the lateral bank of IPS as the "ventral band" (VB). At a high magnification, many somata and radially directed apical dendrites stained by SMI-32 antibody were observed in layers II/III (Fig. 2C, bottom left). At a low magnification, the thickness of the dark band of SMI-32 immunoreactivity occupied more than the half of the full width of the supragranular layers (Fig. 2C, bottom middle). On the other hand, at the more dorsal portion of the lateral IPS (indicated by dotted line in Fig. 2A), although the somata and bundle of dendrites stained by SMI-32 antibody were observed in layers II/III at a high magnification (Fig. 2C, middle left), the relative thickness of the band of SMI-32 immunoreactivity to the full width of the supragranular layers was small (Fig. 2C, center). These observations suggest that the relative thickness of VB can be a histological landmark of the ventral portion of the lateral IPS. Thus, we calculated the relative thickness of VB in layers II/III (indicated by a in the bottom right panel of Fig. 2C) to the full width of the supragranular layers (indicated by b in the bottom right panel of Fig. 2C) using the binarized images, and plotted it against the rostrocaudal levels (solid lines in Fig. 3B, a). VB was observed in a small cortical region of several millimeters along the rostrocaudal axis. The caudal border of VB was the branching point of IPS from the parieto-occipital sulcus (POS), and the rostral border was the point where the annectant gyrus disappeared (Fig. 3A, b). We reconstructed the location of recording sites of all 3DCS cells and compared them with the rostrocaudal extent of the cortical region with VB. As shown in Fig. 3B, all 3DCS cells were recorded from the cortical region characterized by VB in both hemispheres. Neither a 3DCS cell nor a VR cell was recorded from the dorsal half of the lateral bank of IPS (around the thin arrows in Fig. 3A, a, b). These results indicate that VB can be a salient histological landmark of the cortical region from which 3DCS cells are recorded. These observations also suggest that LOP in the caudal IPS defined by Lewis and Van Essen (2000) may be homologous to CIP.

We investigated whether CIP/LOP is histologically distinct from its rostral neighbor LIP. It has been shown that LIP can be divided into two subdivisions: LIPd and LIPv. LIPv is the ventral portion of LIP, which is separated from LIPd by dense myelination (Blatt et al., 1990). We found that CIP and

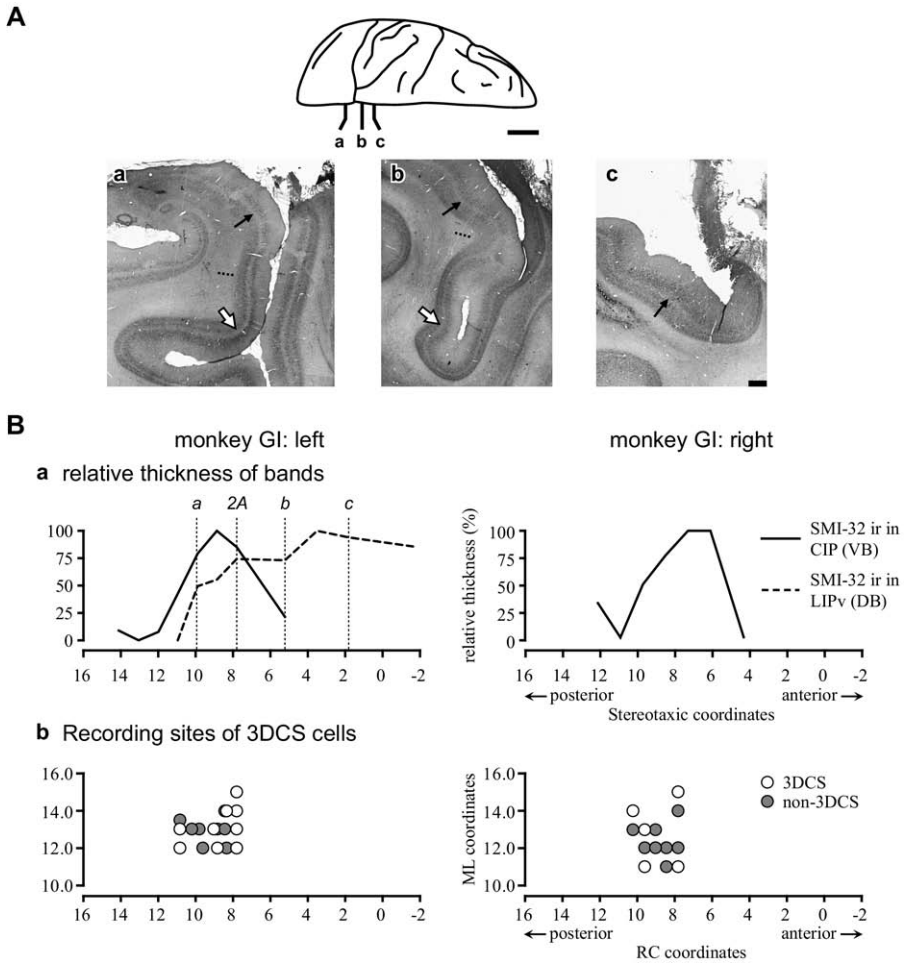

Fig. 3. (A) Coronal sections showing SMI-32 immunoreactivity at three rostrocaudal (RC) levels along the left IPS of monkey GI. The positions of the three sections are indicated in the inset. (a) VB is observed in the "operculum" of the lateral bank of IPS, while DB is also visible at the dorsal part of the bank. These bands were separated by the transitional zone. (b) Caudal border of VB. (c) The intensity of SMI-32 immunoreactivity of DB increased in the rostral direction along IPS, and it merged into the dense band of SMI-32 immunoreactivity characterizing LIPv. There was no indication suggesting that VB merged into DB. Same conventions as those in Fig. 1A. Scale bar=1 mm; 1 cm in inset. (B) (a) Changes in the relative thickness of the bands of SMI-32 immunoreactivity to the full width of the supragranular layers were plotted against the stereotaxic coordinates in the RC direction. The solid and broken lines indicate VB and DB, respectively. The RC levels of sections in Figs. 2A, and a, b, and c in D are indicated by 2A, a, b, and c, respectively. (b) recording sites of 3DCS (white circle) and non-3DCS (gray circle) cells in CIP. The stereotaxic coordinates of the recording sites in the RC and ML directions are plotted in the abscissa and ordinate, respectively. ML, mediolateral; RC, rostrocaudal.

the caudal portion of LIPv can be observed at different portions of the lateral bank of IPS in the same coronal section. A pale band of SMI-32 immunoreactivity was observed in layers II/III of the dorsal corner of IPS where the sulcus appeared to bend laterally in coronal sections (thin arrow in Fig. 2A). To contrast to VB, we refer to this region as the "dorsal band" (DB). At a high magnification, the somata and dendrites extending to the superficial layer stained by SMI-32 antibody were observed in layers II/III (Fig. 2C, top left). At a low magnification, the relative thickness of DB to the full width of the supragranular layers increased as compared with those observed in the transitional zone between DB and VB (Fig. 2C, top middle). The SMI-32 immunoreactivity of DB increased in the rostral direction along IPS, and merged with the dense SMI-32 immunoreactivity in the ventral portion of the lateral IPS, which characterizes LIPv (Fig. 3A). The relative thickness of DB to the full width of the supragranular layers was plotted against the rostrocaudal levels (dotted line in Fig. 3B, a). DB and VB are present within a certain range of the cortical region in the rostrocaudal direction. There was no indication that VB merged with DB. These observations suggest that VB and DB can be histological landmarks of different cortical areas in the lateral IPS.

Unfortunately, we were not able to trace the anterior portion of DB in the right hemisphere of this monkey, because a portion of the brain tissue in our sample was damaged by penetrations of electrodes for long-term neuronal recordings resulting in bleeding. Therefore, we examined SMI-32 immunoreactivity in the caudal IPS of another three monkeys in which no physiological recording was performed. Coronal sections showing SMI-32 immunoreactivity at three different rostrocaudal levels for the three monkeys are shown in Fig. 4A–C. The changes in

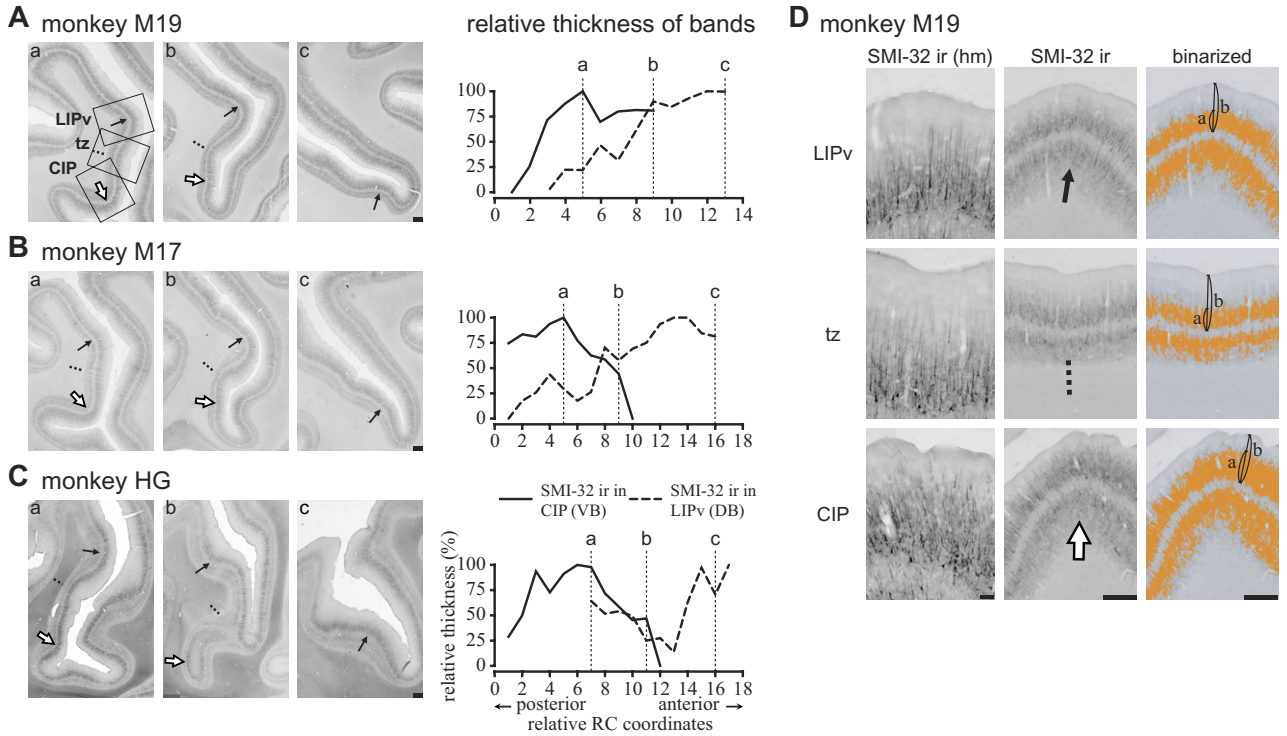

Fig. 4. Photomicrographs showing SMI-32 immunoreactivity and the changes in the relative thickness of VB and DB in three other monkeys (A–C). Same conventions as those in Fig. 2A for photomicrographs and in 3B for the changes in the relative thickness of the bands. The abscissa of the graphs is indicated by relative coordinates in the RC direction. (D) Photomicrographs of SMI-32 immunoreactivity in monkey M19 shown in (A, a). Same conventions as those in Fig. 2C. Scale bar=1 mm in (A−C) and the middle and right columns in (D); 100 μm in the left column in (D).

the relative thickness of VB and DB to the full width of the supragranular layers in these three monkeys were calculated similarly to those in monkey GI using binarized images (Fig. 4D, middle and right columns for monkey M19). In all cases, DB (thin arrows in Fig. 4A–C) was clearly observed in a portion different from that of VB (white arrows) in the same coronal sections, and merged into LIPv in the rostral portion of IPS. These results suggest that CIP may be a cortical area histologically distinct from LIP.

DISCUSSION

3D curvature-selective cells in CIP

In the present study, we investigated (1) whether CIP cells selectively respond to 3D curvatures and (2) whether CIP has any histological property. Regarding the first issue, we found that CIP cells selectively respond to the shape of 3D curvatures. The CPSIs at two levels of curvedness matched well in 3DCS cells. Responses of these cells to the front parallel plane and small disparity patches presented at the positions close to those around the fixation target of preferred stimuli were also tested. However, we were not able to find any modulation by these stimuli in responses of 3DCS cells. Moreover, the local disparity at any point on the surface of the 3D curvatures varied with the stimulus presented. These results indicate that the responses of these cells do not depend on the local disparity of visual stimuli. Out of nineteen 3DCS cells, six (31.6%) showed modulation by both shape index and curvedness. This suggests that the 3D curvatures of a particular shape and curvedness may be represented in CIP. On the other hand, 13 cells (68.4%) showed modulation by only shape index. This indicates that these cells responded equally to a particular shape of curvatures at different curvedness levels, suggesting that an abstract shape of curvatures independent of the amount of curvature may also be encoded in CIP. These results strongly suggest that CIP is an important cortical area for the processing of 3D curvatures.

Studies of computational theory led to the proposal that information of axes and surfaces can be reconstructed by integrating local disparities, and that the surface orientations of planes and curvatures are crucial for the representation of 3D shapes (Marr, 1982). In this study, we found that six cells showed a significant main effect of curvedness only. Although we did not investigate the properties of these cells in detail, it is possible that these cells encode local disparities. Furthermore, previous studies have revealed that CIP cells selectively respond to the axis orientation (Kusunoki et al., 1993; Sakata et al., 1999) and surface orientation (Taira et al., 2000). In particular, CIP cells selectively respond to the surface orientation defined by monocular depth cues including linear perspective (Tsutsui et al., 2001) and texture gradient (Tsutsui et al., 2002) as well as binocular disparity, suggesting that information on monocular and binocular depth cues may be

integrated in CIP. Together with the results of this study, these findings are in line with the theoretical considerations mentioned above, and suggest that CIP may play a crucial role in the processing of 3D structures of objects. These results also suggest that 3D geometrical objects, such as spheres, cubes, cones, and tori may be represented in CIP. A recent functional imaging study of monkeys revealed that cortical regions in the posterior and anterior IPS selectively respond to 3D shapes (Durand et al., 2007).

SMI-32 immunoreactivity

SMI-32 antibody has been shown to recognize a nonphosphorylated epitope of the heavy neurofilament polypeptide in perikarya and dendrites (Sternberger and Sternberger, 1983; Goldstein et al., 1987). This antibody specifically stains a subpopulation of pyramidal cells in layers III and V providing corticocortical projections (Campbell et al., 1991). It has been shown that the pattern of immunohistochemical staining by SMI-32 antibody matches cortical subdivisions defined by cytoarchitecture. Thus, SMI-32 antibody has been used as a marker to parcellate cortical subdivisions in the macaque brain along with antibodies against calcium-biding proteins including parvalbumin, calbindin, and calretinin (Saleem and Logothetis, 2007 and references therein). It has been established that cortical areas in IPS of the macaque monkey are characterized by myeloarchitectonical organization (Blatt et al., 1990). However, myelin staining is a time-consuming technique requiring much skill to obtain clear preparations. On the other hand, immunohistochemical staining with SMI-32 has some advantages over myelin staining. First, the procedure of SMI-32 staining is easier than that of myelin staining. Second, stable staining can be obtained with both the fixatives formalin and paraformaldehyde. Third, SMI-32 staining can be applied to old tissues preserved in a fixative for a long time. If chemoarchitectonic organization by SMI-32 staining is established in IPS, it should provide a useful tool for investigation of the functional and histological properties of this region.

Lewis and Van Essen (2000) investigated subdivisions in the posterior parietal cortex of the macaque monkey by Nissl and myelin stainings, and immunohistochemical staining with SMI-32 antibody. They found that the ventral portion of the lateral bank of the caudal IPS was characterized by dense myelination, and that the density of myelination correlated with SMI-32 immunoreactivity in layers III and V. They designated this region as LOP. In the present study, we confirmed the presence of a dense SMI-32 immunoreactivity in the ventral portion of the lateral bank of the caudal IPS (ventral band, VB), and that all recording sites of 3DCS cells were in the cortical region including VB. These results suggest that LOP identified by Lewis and Van Essen (2000) is homologous to CIP, and that VB can be an anatomical landmark of CIP.

In the caudal part of IPS, another SMI-32 immunoreactive region was observed in the dorsal portion of IPS where the fissure of the sulcus bent laterally in coronal sections (dorsal band, DB). No 3DCS cell was recorded from the cortical region including DB. DB merged into LIPv in more rostral IPS where the fissure of IPS appears straight in coronal sections. This indicates that DB is the caudal portion of LIPv. In the caudal IPS, DB was separated from VB by the cortical region including a thin band of SMI-32 immunoreactivity, and we were not able to find any evidence suggesting that VB was transferred to DB as it goes rostrally along IPS. These findings strongly suggest that CIP/LOP is a cortical area histologically distinct from LIP.

There was variability in the intensity of SMI-32 immunohistochemical staining in animals used in this study, particularly, between the intensity in monkey GI and that in monkeys M17 and M19. As described in the experimental procedures, a portion of the brain tissue of monkey GI was damaged by the neuronal recordings resulting in bleeding. This might result in an artificially low intensity of SMI-32 staining around the damaged tissues. Because the purpose of this study was to compare the patterns of SMI-32 staining with the recording sites of 3DCS cells in the caudal IPS, we allowed a longer time for DAB reaction in the processing of histological samples from monkey GI to obtain intense SMI-32 immunohistochemical staining. To eliminate the effects of variability in the staining across animals, the relative thickness of the bands to the full width of the supragranular layers were normalized to the maximum and minimum values for each animal. It is noteworthy that a similar trend is observed in the changes in the relative thickness of the bands across the four monkeys regardless of the variability in the intensity of SMI-32 immunohistochemical staining. These results suggest that immunohistochemical properties observed in monkey GI are not artifacts but consistent with those in other monkeys.

Functional and anatomical dissociations between CIP and LIP

It has been shown that LIP is involved in the visuomotor control of eye movements (Sakata et al., 1980; Barash et al., 1991a,b; Colby et al., 1996). Anatomically, it has been shown that LIP has strong neuronal connections with the frontal eye field (Andersen et al., 1990). In contrast, cells that selectively respond to 3D structures were recorded from a cortical region different from that where cells showing saccade-related activity were observed. This selectivity was used to discriminate CIP from LIP in early studies (M. Kusunoki, MRC Cognition and Brain Sciences Unit, Cambridge, UK, personal communication). Recently, we have demonstrated by injection of neuronal tracers into CIP that CIP has weak connections with area 8A (Katsuyama et al., 2008). These findings suggest that neuronal connections of CIP with other cortical areas may be different from those of LIP depending on their functional dissociations. Anatomical studies have revealed that CIP receives inputs from V3A and sends projections to AIP (Nakamura et al., 2001), which sends projections to the ventral premotor area (Matelli et al., 1986). It has been revealed that cells in AIP and the ventral premotor area show activity related to movements of hand-manipulation of 3D objects (Rizzolatti et al., 1988; Sakata et al., 1998). These findings suggest that CIP plays an important role in the visuomotor control system by providing visual information on the 3D structure of

objects. On the other hand, CIP may be involved in the perception of 3D objects *per se*, because CIP cells show a delayed activity in response to the surface orientation during the delayed-matching-to-sample task (Tsutsui et al., 2003).

CONCLUSION

We showed that cells in CIP of the macaque monkey selectively responded to 3D curvatures, suggesting that CIP may be a crucial cortical area for the perception of 3D shapes. Our immunohistochemical study showed that all the recording sites of 3DCS cells were located in a small cortical region with a dense band of SMI-32 immunoreactivity. This region was spatially separated from LIPv, which also showed a band of SMI-32 immunoreactivity. These results suggest that CIP may be homologous to LOP designated to be in the caudal IPS by Lewis and Van Essen (2000), and that CIP may be a cortical area distinct from LIP histologically as well as functionally.

Acknowledgments—The authors thank Drs. Masahiko Takada, Shigehiro Miyachi, and Daisuke Takahara for kindly providing us with the samples for immunohistochemistry. This study was supported by the Academic Frontier Project at Nihon University: a matching fund subsidy from MEXT and Grants-in-Aid for Scientific Research on Priority Areas from the Ministry of Education, Culture, Sports, Science and Technology of Japan (#17022038).

REFERENCES

Andersen RA, Asanuma C, Essick G, Siegel RM (1990) Corticocortical connections of anatomically and physiologically defined subdivisions within the inferior parietal lobule. J Comp Neurol 296:65–113.

Barash S, Bracewell RM, Fogassi L, Gnadt JW, Andersen RA (1991a) Saccade-related activity in the lateral intraparietal area. I. Temporal properties; comparison with area 7a. J Neurophysiol 66: 1095–1108.

Barash S, Bracewell RM, Fogassi L, Gnadt JW, Andersen RA (1991b) Saccade-related activity in the lateral intraparietal area. II. Spatial properties. J Neurophysiol 66:1109–1124.

Blatt GJ, Andersen RA, Stoner GR (1990) Visual receptive field organization and cortico-cortical connections of the lateral intraparietal area (area LIP) in the macaque. J Comp Neurol 299:421–445.

Campbell MJ, Hof PR, Morrison JH (1991) A subpopulation of primate corticocortical neurons is distinguished by somatodendritic distribution of neurofilament protein. Brain Res 539:133–136.

Colby CL, Duhamel JR, Goldberg ME (1996) Visual, presaccadic, and cognitive activation of single neurons in monkey lateral intraparietal area. J Neurophysiol 76:2841–2852.

de Vries SC, Kappers AM, Koenderink JJ (1993) Shape from stereo: a systematic approach using quadratic surfaces. Percept Psychophys 53:71–80.

Durand JB, Nelissen K, Joly O, Wardak C, Todd JT, Norman JF, Janssen P, Vanduffel W, Orban GA (2007) Anterior regions of monkey parietal cortex process visual 3D shape. Neuron 55: 493–505.

Goldstein ME, Sternberger LA, Sternberger NH (1987) Varying degrees of phosphorylation determine microheterogeneity of the heavy neurofilament polypeptide (Nf-H). J Neuroimmunol 14:135–148.

Isoda M, Tsutsui K, Katsuyama N, Naganuma T, Saito N, Furusawa Y, Mushiake H, Taira M, Tanji J (2005) Design of a head fixation device for experiments in behaving monkeys. J Neurosci Methods 141:277–282.

Katsuyama N, Yamashita A, Sato N, Usui N, Taira M (2008) Anatomical dissociation of CIP and LIP in the macaque intraparietal cortex. In: Society of Neuroscience Abstract 853.13/EE1; 2008; Washington, DC.

Koenderink JJ (1990) Solid shape. Cambridge: MIT Press.

Kusunoki M, Tanaka Y, Ohtsuka H, Ishiyama K, Sakata H (1993) Selectivity of the parietal visual neurons in the axis orientation of objects in space. Soc Neurosci Abstr 19:770.

Lewis JW, Van Essen DC (2000) Mapping of architectonic subdivisions in the macaque monkey, with emphasis on parieto-occipital cortex. J Comp Neurol 428:79–111.

Marr D (1982) Vision: a computational investigation into the human representation and processing of visual information. San Francisco: W.H. Freeman.

Matelli M, Camarda R, Glickstein M, Rizzolatti G (1986) Afferent and efferent projections of the inferior area 6 in the macaque monkey. J Comp Neurol 251:281–298.

Nakamura H, Kuroda T, Wakita M, Kusunoki M, Kato A, Mikami A, Sakata H, Itoh K (2001) From three-dimensional space vision to prehensile hand movements: the lateral intraparietal area links the area V3A and the anterior intraparietal area in macaques. J Neurosci 21:8174–8187.

Prince SJD, Pointon AD, Cumming BG, Parker AJ (2002) Quantitative analysis of the response of V1 neurons to horizontal disparity in dynamic random-dot stereograms. J Neurophysiol 87:191–208.

Rizzolatti G, Camarda R, Fogassi L, Gentilucci M, Luppino G, Matelli M (1988) Functional organization of inferior area 6 in the macaque monkey. II. Area F5 and the control of distal movements. Exp Brain Res 71:491–507.

Sakata H, Shibutani H, Kawano K (1980) Spatial properties of visual fixation neurons in posterior parietal association cortex of the monkey. J Neurophysiol 43:1654–1672.

Sakata H, Taira M, Kusunoki M, Murata A, Tanaka Y, Tsutsui K (1998) Neural coding of 3D features of objects for hand action in the parietal cortex of the monkey. Philos Trans R Soc Lond B Biol Sci 353:1363–1373.

Sakata H, Taira M, Kusunoki M, Murata A, Tsutsui K, Tanaka Y, Shein WN, Miyashita Y (1999) Neural representation of three-dimensional features of manipulation objects with stereopsis. Exp Brain Res 128:160–169.

Saleem KS, Logothetis NK (2007) A combined MRI and histology: atlas of the rhesus monkey brain in stereotaxic coordinates. London: Academic Press.

Sternberger LA, Sternberger NH (1983) Monoclonal antibodies distinguish phosphorylated and nonphosphorylated forms of neurofilaments in situ. Proc Natl Acad Sci U S A 80:6126–6130.

Taira M, Tsutsui K, Jiang M, Yara K, Sakata H (2000) Parietal neurons represent surface orientation from the gradient of binocular disparity. J Neurophysiol 83:3140–3146.

Tsutsui K, Jiang M, Yara K, Sakata H, Taira M (2001) Integration of perspective and disparity cues in surface-orientation-selective neurons of area CIP. J Neurophysiol 86:2856–2867.

Tsutsui K, Sakata H, Naganuma T, Taira M (2002) Neural correlates for perception of 3D surface orientation from texture gradient. Science 298:409–412.

Tsutsui K, Jiang M, Sakata H, Taira M (2003) Short-term memory and perceptual decision for three-dimensional visual features in the caudal intraparietal sulcus (area CIP). J Neurosci 23:5486–5495.

(Accepted 14 January 2010)
(Available online 20 January 2010)